Time-Reversal: Spatio-temporal focusing and its dependence on channel correlation

Persefoni Kyritsi, and George Papanicolaou

***Abstract*— We study a wireless communications system that applies time reversal to transmit the desired signal, so that it focuses spatially and compresses temporally on the intended receiver. Our theoretical calculations relate the achievable temporal and spatial compression to the channel propagation characteristics and the number of transmit antennas. We validate our theoretical results with extensive simulations using the 802.11n channel model. The results verify the theory that temporal and spatial focusing depend strongly on the product of the delay spread and the bandwidth, as well as the angular characteristics of the channel. We show that, because of spatial focusing at the intended receiver, this system has a low probability of intercept.**

***Index Terms*— Wireless communications, time reversal, delay spread, spatial focusing.**

I. Introduction

TIME reversal (TR) is a method to focus spatially and compress temporally broadband signals through a richly scattering environment [1], [2]. It involves two stages. In the first stage (channel estimation stage), a source emits a short pilot signal. This signal propagates in a richly scattering medium. Its response is recorded by each element of an array that will act as a transmitter in the data transmission stage. The duration of each of these recorded signals is significantly longer than the initial pilot pulse due to multiple scattering. The second stage is the actual data transmission. In this stage, all the elements of the transmitter array send the same data stream, and each one filters the signal to be transmitted through a *time-reversal filter*, *i.e.* a filter that has a form similar to the signal recorded at that particular element during the channel estimation stage, reversed in time (the first portion recorded becomes the last portion transmitted). These transmitted signals focus sharply in space and compress tightly in time at the source location. Moreover, they do so robustly.

Extensive laboratory TR experiments have shown this spatial focus and temporal compression across a broad range of settings in ultrasound experiments (see [3] and references contained within). In each of these experiments, spatial focusing and temporal compression occur robustly.

Much research activity has been dedicated to using TR for multiple-input/single-output (MISO) underwater communication systems. In fact, several experiments in the ocean have demonstrated MISO-TR communications to be feasible [4], [9]–[12].

Recently, there has been an effort to apply the principle of TR to electromagnetic waves at radio frequencies. The first experimental demonstration showed that indeed it is possible to achieve temporal compression of wideband signals that are transmitted over the radio channel [5]. A different experiment illustrated the spatial focusing properties of TR for electromagnetic waves using a narrowband system [27]. The post-processing of wideband fixed wireless access channel measurements showed that it is indeed possible to reduce the delay spread of the channel, by using conventional TR or advanced weighting schemes [7], [8]. Moreover, post-processing of ultra wideband measurements illustrated the spatial focusing potential of a TR system that employs a single transmit antenna [24].

Temporal focusing is a desired property because it provides a method to reduce intersymbol interference (ISI). Commonly such an issue is addressed by increasing the receiver complexity using advanced equalization or multi-carrier schemes (*i.e* OFDM). Hence, a TR communication system with low ISI would reduce the required complexity at the receiver.

Spatial focusing on the intended receiver is also a desirable property because it indicates that the communications system has a low probability of intercept (LPI) by another receiver located nearby [17]. Statistical robustness is also a desirable property because it indicates that the system does not suffer from fading.

In this paper we study the advantages gained by MISO-TR communication in terms of temporal and spatial focusing and relate them to the channel propagation properties and the system size, under the following assumptions:

- The elements of the transmitting array have perfect Channel State Information (CSI), *i.e.* there is no noise in the channel estimation stage.
- The channel is stationary, *i.e.* it is the same during both stages of the TR process.

We also show the statistical robustness of these properties.

For our numerical simulations, we implement the 802.11n channel model that is applicable for systems with bandwidth up to 100MHz around either 2.5 or 5GHz. We validate the theoretical results and demonstrate that the key parameters are the delay spread (DS) [14] and the angular spread of the channel. Moreover, we show that the implementation of a MISO-TR system results in low signal levels around the intented receiver, and therefore makes it hard for an eavesdropper to intercept the content of the communication. This property is referred to as Low Probability of Intercept

Manuscript Draft: May 24, 2005

P. Kyritsi is a Visiting Researcher at the Department of Mathematics of Stanford University, Stanford, CA 94305-2125, and an Assistant Research Professor at the Department of Communication Technology of Aalborg University, Aalborg, Denmark (email: kyritsi@math.stanford.edu)

G. Papanicolaou is a Professor at the Department of Mathematics of Stanford University, Stanford, CA 94305-2125, USA (email: papanico@math.stanford.edu)

(LPI). For example, our simulation results show that at a distance of one wavelength away from the intended receiver, the received power is lower than the power on the intended receiver by 10dB.

The remainder of this paper is organized as follows. In Section II we discuss a TR system. In Section III we discuss the channel model that is used for our simulations. In Section IV we show the theoretical results that govern temporal and spatial focusing. Section V shows the results of the simulations and the effect of the various parameters that affect spatial/ temporal focusing and the robustness of TR. The conclusions are in Section VII.

II. System Description

Lower case letters indicate function in time, whereas upper case letters are used for their frequency representation. Bold letters indicate vectors, $\overline{(\cdot)}$ denotes the complex conjugate of the argument $(\cdot)$, and $\otimes$ denotes the convolution operator. We look at the analytic representation of the signals and therefore consider them to have spectral content in $[-B/2, B/2]$, where B is the system bandwidth. The actual communication occupies the spectrum $[f_c - B/2, f_c + B/2]$ around the carrier frequency f_c. In the following we denote as $h(t; \mathbf{r}_{TX}, \mathbf{r}_{RX})$ the channel impulse response from a transmitter at location $\mathbf{r}_{TX}$ to a receiver at location $\mathbf{r}_{RX}$.

We describe the operation of a downlink communications system with N_{TX} transmit antennas as a two-stage process.

A. Fundamentals of TR Systems

We distinguish two stages in the operation of a downlink TR system with N_{TX} transmit antennas. The first stage is the *channel estimation*, and the second stage is the *data transmission*.

1) Channel estimation: The first stage is the channel estimation stage, during which each element of the transmit array obtains knowledge of the channel impulse response (CIR) to the intended receiver. There are several ways in which channel estimation can be implemented:

- The intended receiver (Rx) sends a pilot signal, and each element in the transmitting array (Tx) records the convolution of this pilot signal with the CIR. Due to the reciprocity of the channel, this is also the CIR from that transmit array element to the intended receiver. This approach can be used in time domain duplex (TDD) systems, where the ends of the communication link take turns in sending data.
- The transmitters send training sequences or pilot symbols, and the intended receiver estimates the CIR from each transmitting element. It then feeds back this information to the Tx array. This approach is more suitable for frequency domain duplex (FDD) systems where uplink and downlink communications occupy different parts of the radio spectrum.

In both cases, the accuracy of the channel state information (CSI) at the transmitter depends on the implementation details of the channel estimation, the noise during that process, its repetition rate and the rate of change of the channel. In this paper, we are not concerned with the specifics of the channel estimation and assume that the transmitter has perfect and instantaneous CSI.

2) Data transmission: The second stage is the actual data transmission. The Tx uses the CSI it acquired during the channel estimation stage to transmit a bitstream that focuses spatially and is compressed temporally on the Rx. Each of the N_{TX} elements of the transmit array transmits simultaneously the same signal $x(t)$, by filtering it through the time reversed and phase conjugated version of its CIR to the intended receiver. Let the baseband representation of the signal $x(t)$ to be transmitted be given by

$$x(t) = \sqrt{P} \sum_{k=-\infty}^{\infty} \beta_k \delta(t - kT_s) \tag{1}$$

where P is the transmitted power, and T_s is the symbol time. It denotes the time by which consecutive symbols β_k are separated. It is related to the bandwidth B of the system and the pulse shaping that is used. Namely, the T_s should be greater or equal than $1/B$. The quantity β_k denotes the mapping of the data stream b_k that is destined for the user at $\mathbf{r}_{RX}$ for the modulation scheme used. The constellation points are selected so that $E[|\beta_k|^2] = 1$ in order for the transmit power to be determined by P.

If $g_m(t)$ is the filter at the m-th transmit antenna, then

$$g_m(t) = A \cdot \overline{h(-t; \mathbf{r}_{Txm}, \mathbf{r}_{RX})} \tag{2}$$

$\mathbf{r}_{TX_m}$ is the location of the m-th transmit antenna. The scaling factor A is determined so that the TR filters do not introduce any signal amplification. It is irrelevant for our analysis and we therefore drop it from our notation.

If we look at the equivalent frequency domain representation of the signals, TR describes the situation where each transmitter modulates the spectrum $X(f)$ of $x(t)$ with the phase-conjugated spectrum of the channel transfer function $H(f; \mathbf{r}_{TX_m}, \mathbf{r}_{RX})$.

The received signal at the Rx is $y(t)$ and can be written as

$$y(t) = \left(\sum_{m=1}^{N_{Tx}} h(t; \mathbf{r}_{TX_m}, \mathbf{r}_{RX}) \otimes \overline{h(-t; \mathbf{r}_{Txm}, \mathbf{r}_{RX})} \right) \otimes x(t) + n(t), \tag{3}$$

where $n(t)$ is the receiver noise, assumed to be additive white Gaussian noise.

We define the equivalent channel impulse response $h_{eq}(t)$ as

$$h_{\text{eq}}(t) = \sum_{m=1}^{N_{Tx}} h(t; \mathbf{r}_{TX_m}, \mathbf{r}_{RX}) \otimes \overline{h(-t; \mathbf{r}_{TX_m}, \mathbf{r}_{RX})}. \tag{4}$$

It is interesting to point out that the equivalent channel impulse response is given as the sum of the autocorrelations of the CIRs to the individual array elements. Therefore it is symmetric around $t = 0$, and achieves its maximum at $t = 0$. This determines the synchronization between Tx and Rx, as well as the sampling time at the Rx.

In the frequency domain, the equivalent channel transfer function $H_{\text{eq}}(f)$ can be written as

$$H_{\text{eq}}(f) = \sum_{m=1}^{N_{Tx}} H_m(f)\overline{H_m(f)} = \sum_{m=1}^{N_{TX}} |H_m(f)|^2. \quad (5)$$

The inherent assumption in the formulation above is that the channel transfer functions have not changed in the data transmission stage relative to the channel estimation stage. This simplification is valid in slowly varying environments, or when the channel estimation is repeated and the channel state information is updated frequently. The effect of time-varying channels is beyond the scope of this paper.

By the properties of TR in richly scattering media, the signal $y(t)$ is expected to focus spatially at the Rx and compress temporally.

B. Temporal focusing

The common measure for the temporal extent of the CIR is the delay spread (DS), which is defined as the second central moment of the channel power delay profile $pdp(\tau)$:

$$DS^2 = \frac{1}{\int_{-\infty}^{+\infty} pdp(\tau)d\tau} \int_{-\infty}^{+\infty} (\tau - \bar{\tau})^2 \, pdp(\tau)d\tau \quad (6)$$

where

$$pdp(\tau) = E\left[|h(\tau)|^2\right] \quad (7)$$

$$\bar{\tau} = \frac{1}{\int_{-\infty}^{+\infty} pdp(\tau)d\tau} \int_{-\infty}^{+\infty} \tau pdp(\tau)d\tau \quad (8)$$

The power delay profile is calculated as the expected value of the power of the CIR within the local area of the transmitter/ receiver.

It has been shown that large delay spread leads to irreducible bit error rate (BER), [20], which means that at high signal to noise ratios, intersymbol interference (ISI) becomes the dominant impairment in the data detection. Therefore delay spread is a fundamental limitation for wireless systems, and is more severe as the bandwidth of the signals of interest increases. In order to combat ISI in large delay spread channels, several techniques have been proposed. For example, CDMA systems exploit the delayed channel taps with a rake receiver, and OFDM systems separate the bandwidth into several narrow bands over which the delay spread appears to be negligible. Such multi-carrier schemes come at a cost of advanced processing at the receiver and possibly the transmitter.

We choose to concentrate on a different framework wherein the receivers are as simple as possible. We allow however for advanced system complexity at the tranmsitter. Our purpose is to exploit CSI at the transmitter and reduce the perceived delay spread at the receiver. To that end, we investigate the perceived delay spread that can be achieved after the application of TR at the transmitter.

C. Spatial Focusing

Let us assume that the system performs TR with a view to communicating with an intended receiver that is located at $\mathbf{r}_{RX}$. We are interested in the amount of interference this operation causes at a location at distance $\mathbf{d}$ away from the intended receiver, *i.e.* at a location $\mathbf{r}' = \mathbf{r}_{RX} + \mathbf{d}$. The reason for this is two-fold:

1) Low interference power at location $\mathbf{r}'$ would mean that it would be possible to simultaneously send data to both locations $\mathbf{r}$ and $\mathbf{r}'$, without impairing each individual communications link. Therefore it impacts the system capacity.
2) The received power away from the target is a measure of the system's probability of intercept: low power at a distance $\mathbf{d}$ away from the intended receiver indicates that an eavesdropper at that location would not be able to successfully intercept the content of the communication.

We are interested in the spatial distribution of the interference, and therefore look at the equivalent channel impulse response at location $\mathbf{r}'$.

$$h_{\text{eq}}(t;\mathbf{r}') = \sum_{m=1}^{N_{Tx}} h(t;\mathbf{r}_{TX_m},\mathbf{r}') \otimes \overline{h(-t;\mathbf{r}_{TX_m},\mathbf{r}_{RX})} \quad (9)$$

where $h(t;\mathbf{r}_{TX_m},\mathbf{r}')$ indicates the channel impulse response from the m-th transmitter to $\mathbf{r}'$.

Assuming a perfectly synchronous system, and keeping in mind that the equivalent channel impulse response on the intended receiver achieves its maximum at $t = 0$, we concentrate on the value of the interference at that sampling instant, *i.e.* we are interested in

$$IF(\mathbf{r}') = h_{\text{eq}}(0;\mathbf{r}') \quad (10)$$

In [17], the spatial peak-to-sidelobe ratio was used to determine the quality of the spatial focusing. In our case, we look at the overall distribution of the interference.

III. Channel model

In the following, we give a brief description of the principles that underlie the 802.11n channel model, which will be used for our simulations. Details can be found in [22].

A. Tap delay line model

The channel impulse response of a wideband system can be expressed as a tap delay line model with L taps of the form

$$h(\tau) = \sum_{l=0}^{L-1} h_l \delta(\tau - \tau_l) \quad (11)$$

The l-th tap has complex amplitude h_l and arrives at delay τ_l, and taps that arrive at different delays are assumed to be uncorrelated. For simplicity, we assume that the delays $\tau_l = lT_u$ are the integer multiples of the same time unit T_u for $l = 0, \ldots, L-1$, *i.e.* $\tau_l = lT_u$.

The tap amplitudes follow a known power delay profile pdp

$$E[|h_l|^2] = pdp(\tau_l) = P_l \quad (12)$$

Using this description, it is possible to have $P_l = 0$ for some values of l.

The minimum tap spacing relates to the system bandwidth B that the model characterizes. Namely it cannot be above $1/B$.

The statistical distribution of the tap amplitudes depends on the propagation conditions. In this paper we investigate the case where the amplitudes h_l are Rayleigh distributed [16].

Let $h_{l,I}$, $h_{l,Q}$ denote the in-phase and quadrature components of h_l respectively. The Rayleigh distribution reflects the case where each tap is the sum of several irresolvable paths, and therefore $h_{l,I}$, $h_{l,Q}$ are independent, identically distributed zero-mean Gaussian random variables with variance $E\left[\left|\, h_l \,\right|^2\right]/2 = P_l/2$.

B. Correlation and power azimuth spectrum

The cross-correlation between the waves impinging on two antenna elements has been studied in various references, and it has been shown to be a function of the Power Azimuth Spectrum (PAS) and the radiation pattern of the antenna elements. Antenna elements will be assumed to be omnidirectional in the following.

We define the random variables

$$\begin{aligned} x &= x_I + j \cdot x_Q = h_l(\mathbf{r}) \\ y &= y_I + j \cdot y_Q = h_l(\mathbf{r} + \mathbf{d}) \end{aligned} \tag{13}$$

x, y denote the complex amplitude of the l-th tap at locations $\mathbf{r}$ and $\mathbf{r}' = \mathbf{r} + \mathbf{d}$ respectively. x_I, y_I denote the in phase components of x, y respectively, and x_Q, y_Q denote the quadrature components of x, y respectively.

For Rayleigh channels, it can easily be shown that the following properties hold for the correlations of x_R, y_I, x_Q, y_Q [19]:

$$R_{x_I y_I} = R_{x_Q y_Q} \tag{14}$$

$$R_{x_I y_Q} = -R_{x_Q y_I} \tag{15}$$

The complex correlation of x, y is given by

$$\rho = R_{x_I y_I} + j R_{x_I y_Q} \tag{16}$$

The correlations depend on the power azimuth spectrum according to the following equations:

$$R_{x_I y_I}(\mathbf{d}) = \int_{+\pi}^{-\pi} cos\left(kd\cos(\phi - \theta)\right) PAS\left(\phi\right) d\phi \tag{17}$$

$$R_{x_Q y_I}(\mathbf{d}) = \int_{+\pi}^{-\pi} sin\left(kd\sin(\phi - \theta)\right) PAS\left(\phi\right) d\phi \tag{18}$$

The incidence vector $\mathbf{k}$ is defined for a wave impinging from the azimuth direction ϕ, as

$$\mathbf{k} = \frac{2\pi}{\lambda}\left(cos\phi\hat{x} + sin\phi\hat{y}\right) \tag{19}$$

and

$$\mathbf{d} = d\left(cos\theta\hat{x} + sin\theta\hat{y}\right) \tag{20}$$

($\hat{x}$, $\hat{y}$ are the unitary vectors along the x and y directions respectively).

In the limiting case of uniform PAS over $[0, 2\pi]$, the correlation is the well-known zero-th order Bessel function of the first kind. In the more general case, the PAS is characterized by the following characteristics:

1) Shape
   Several distributions have been used to describe the angular spread around the mean angle of incidence. Some of the most popular such distributions are the uniform, the truncated Gaussian and the truncated Laplacian ($PAS(\phi) = Ce^{-\sqrt{2}\frac{|\phi|}{\sigma}}, |\phi| \leq \frac{\Delta\phi}{2}$), that have been shown to fit different sets of experimental data. Specifically the 802.11n channel model assumes that the angles of arrival follow the truncated Laplacian distribution.
2) Number of clusters
   Radio waves gather in clusters distributed over the space domain. Each cluster has different mean angle of incidence and a different spread around it. In our case we assume that each individual cluster exhibits the same inner type of distribution. The spread of each cluster around its mean angle of incidence is allowed to vary from cluster to cluster.

C. Kronecker model

Let $h_l(\mathbf{r}_{TX_m}, \mathbf{r}_{RX_p})$ denote the amplitude of the l-th tap of $h(\tau; \mathbf{r}_{TX_m}, \mathbf{r}_{RX_p})$, *i.e.* of the channel impulse response between a transmitter at $\mathbf{r}_{TX_m}$ and a receiver at $\mathbf{r}_{RX_p}$. Also let $h_l(\mathbf{r}_{TX_n}, \mathbf{r}_{RX_q})$ denote the amplitude of the l-th tap of $h(\tau; \mathbf{r}_{TX_n}, \mathbf{r}_{RX_q})$, *i.e.* of the channel impulse response between a transmitter at $\mathbf{r}_{TX_n}$ and a receiver at $\mathbf{r}_{RX_q}$.

The 802.11n channel model assumes the Kronecker property for the channel correlation, *i.e.* it assumes that the correlation on the transmitting and the receiving sides are separable.

The Kronecker property states that

$$\begin{aligned} \rho^{IQ}(h_l(\mathbf{r}_{TX_m}, \mathbf{r}_{RX_p}), h_l(\mathbf{r}_{TX_n}, \mathbf{r}_{RX_q})) = \\ \rho_{RX}(\mathbf{r}_p - \mathbf{r}_q) \cdot \rho_{TX}(\mathbf{r}_m - \mathbf{r}_n) \end{aligned} \tag{21}$$

i.e. the correlation of $h_l(\mathbf{r}_{TX_m}, \mathbf{r}_{RX_p})$ and $h_l(\mathbf{r}_{TX_n}, \mathbf{r}_{RX_q})$ can be factored into two terms:

1) Receive correlation $\rho_{RX}(\mathbf{r}_p - \mathbf{r}_q)$
   This term involves only the locations of the receivers p, q.
2) Transmit correlation $\rho_{TX}(\mathbf{r}_m - \mathbf{r}_n)$
   This term involves only the locations of the transmitters m, n.

The receive correlations can be intuitively calculated from the PAS around the receiver location (distribution of the angles of arrival (AoA)) as in the previous section.

The calculation of the transmit correlations can be done in a similar fashion. We take into account the reciprocity of the channel, and describe the angular distribution around the transmitter by the distribution of angles of departure (AoD). We then calculate the transmit correlations as in the previous section.

It is interesting to point out the region of validity of the Kronecker model. This channel property has been experimentally validated in a variety of propagation environments [18]. There have also been situations (namely scenarios where propagation is governed by deterministic phenomena such as waveguiding),

where it no longer holds [21]. Such scenarios should be addressed separately and are beyond the scope of this paper. Most importantly, the Kronecker model can be used if and only if the transmitting (receiving) antennas are within the same local area ($\mathcal{O}(10\lambda)$), as would be the case in a multiple element antenna array. It no longer holds for transmit antennas that are separated by large distances (*e.g.* if the transmit elements are placed atop of several spatially separated buildings) and therefore have very different channels to the receiver, both in terms of average received power and in terms of the angular properties.

D. The 802.11n channel model

[22] describes a set of 2-dimensional 802.11n channel models applicable to indoor multiple input- multiple output (MIMO) wireless local area network (WLAN) systems. The channel models are an extension of the single input- single output (SISO) WLAN channel models ([28], [29]) to the multiple antenna case. The 802.11n channel models are based on the cluster model developed by Saleh and Valenzuela [30], which describes a process whereby channel taps arrive clustered in time. The new models also display clustering in angle, a property that has been experimentally demonstrated in various environments (see [32] among others).

The model can be used for both the 2GHz and the 5GHz frequency bands, since the experimental data and published results for both bands were used in its development (average, rather than frequency dependent model). In order for the model to be used for system-wide simulations, the path loss model is specified (*i.e.* the law that determines how the average received power falls off with distance from the transmitter). This is frequency dependent (power falls off faster with distance in the 5GHz case).

The minimum tap spacing in all the models is $T_u = 10ns$. Although the systems that the 802.11n channel models address have a bandwidth $B_{802.11n} = 20$MHz, we can use the model to characterize bandwidths up to $1/T_u = 100$MHz.

The models were developped in a step-wise fashion: In each of the three SISO models (A-C) in [28], distinct clusters are first identified. The number of clusters varies from 2 to 6, depending on the model. Each channel tap is contains power arriving from the direction of one or more clusters, and can therefore be considered as the sum of several independent sub-taps, each corresponding to a different angular cluster. The amount of power of each sub-tap is determined so that the sum of their powers equals the power of the composite tap in the original power delay profile. Next, angular spread (AS), angle-of-arrival (AoA), and angle of departure (AoD) values are assigned to each tap and cluster (using statistical methods) that agree with experimentally determined values reported in the literature. Cluster AS was experimentally found to be in the 20^o to 40^o range, and the mean AoA was found to be random with a uniform distribution. Given the angular properties of each cluster, the number of subtaps that compose each tap and the power that each one of them contributes, the PAS is defined for each tap. The knowledge of the PAS allows as to calculate the correlation of any pair of transmit-receive links, for a given antenna configuration.

In total, there are 6 channel models that correspond to different types of propagation scenarios. A brief description is shown in Table I.

Model	Delay Spread (ns)	Environment	K-factor (dB)
A	0	Reference	0/-∞
B	15	Residential home/ Office	0/-∞
C	30	Residential home/ Office	0/-∞
D	50	Typical office environment	3/-∞
E	100	Typical large open space	6/-∞
F	150	Large open space	6/-∞

TABLE I
802.11N CHANNEL MODELS

Models D-F were derived from the original SISO channel models. The various channel models differ in delay spread and angular spread. The taps are assumed to be Rayleigh distributed. The channel models provide for the case of Ricean fading, by assigning a specific K-factor to the first channel tap in the case of line-of-sight scenarios (assumed to occur up to a break point distance d_{BP}, also specified by the model). The values of the K-factors have been selected so as to match experimental observations and are higher for channels with larger delay spreads.

The simulations developed below are based on the 802.11n channel models as in [22], unless otherwise noted. The simulation code was developed based on the software that accompanies the channel model (details can be found in [23]). The original code calculates the correlation characteristics (and from those the channel transfer function) for a fixed and finite array size at both the transmitting and the receiving end. In our case, the number of transmitters (N_{TX}) is finite. However, we are interested in a local area around the intended receiver. To adapt the original code, we look at a grid of points around the target and place fictitious receive antennas at each point of the grid. The implication is that the size of the computational problem increases significantly: the equivalent number of receive antennas becomes N_xN_y, where N_x, N_y are the grid dimensions (number of grid points) in the $x-, y-$ directions respectively. If $2L_x$ is the total grid size along x, and the point spacing is dx, then $N_x = (2L_x/dx + 1)$. Similarly for the y direction.

In our case, we concentrate on the amount of interference around the intended receiver relative to the power on the target. Therefore we are not interested in the absolute power level on the intended receiver, and do not incorporate the path-loss model. The issue of system wide interference calculation is a topic of further research.

E. Models under study

The channel models that we are going to use for our comparison correspond to Models B and C of the IEEE 802.11n specification.

- Model B: Model B corresponds to the environment of a residential building or a small office. Fig. 1 shows the tap delay line model for this scenario (not normalized to unit total power). The delay spread is $15ns$, and we can clearly distinguish two clusters by visual inspection of the

tap delay line. The cluster parameters are summarized in Table II.

Cluster	1	2
Mean AoA	4.3^o	118.4^o
AS (Rx)	14.4^o	25.2^o
Mean AoD	225.1^o	106.5^o
AS (Tx)	14.4^o	25.4^o

TABLE II
ANGULAR PARAMETERS FOR MODEL B

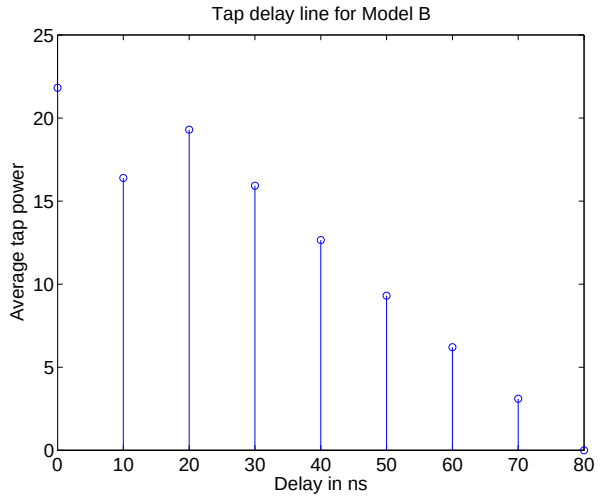

Fig. 1. Tap delay line for Model B

- Model C: Model C also corresponds to the environment of a residential building or a small office. Fig. 2 shows the tap delay line model for this scenario (not normalized to unit total power). In contrast to Model B, the delay spread is $30ns$.

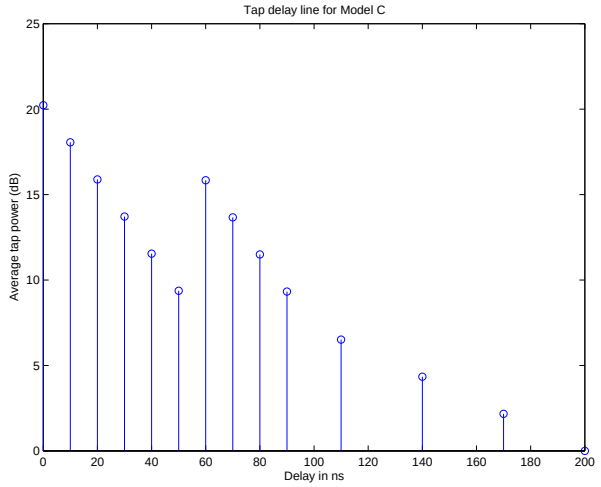

Fig. 2. Tap delay line for Model C

We can again clearly distinguish two clusters by visual inspection of the tap delay line. The original cluster parameters are summarized in Table III.

- Modified Model C: We observe that Model C not only has longer delay spread, but also has wider angular spread than model B. In order to study the effect of the delay spread and the angular spread independently, we introduce a modified model C, that has the same pdp as model C, but the same angular parameters as model B. The tap delay line for this model is going to be like the one shown in Fig. 2, and the angular parameters will be the ones shown in Table II.

Cluster	1	2
Mean AoA	290.3^o	332.3^o
AS (Rx)	24.6^o	22.4^o
Mean AoD	13.5^o	56.4^o
AS (Tx)	24.7^o	22.5^o

TABLE III
ANGULAR PARAMETERS FOR MODEL C

IV. THEORETICAL RESULTS

A. Baseline scenario

Our baseline scenario is communication over the wireless link without any form of preprocessing at the transmitter. The channel to any receiver location $\mathbf{r}$ is given as a tap delay line of the form $h(t;\mathbf{r}) = \sum_{l=0}^{L-1} h_l(\mathbf{r})\delta(t-\tau_l)$, as in equation (11). The l-th tap has complex amplitude h_l and arrives at delay τ_l. The tap amplitudes follow a known power delay profile $pdp(\tau_l) = E[|h_l|^2] = P_l$.

We assume that each receiver performs a matched filtering operation with the corresponding filter $h(t;\mathbf{r})$ in order to detect the transmitted signal. At the sampling instant the received signal power P_{rec} at location $\mathbf{r}$ is

$$P_{rec}(\mathbf{r}) = \sum_{l=0}^{L-1} |h_l(\mathbf{r})|^2. \tag{22}$$

The expected value of the signal power is then

$$E[P_{rec}(\mathbf{r})] = \sum_{l=0}^{L-1} P_l \tag{23}$$

and therefore we expect it to be constant over the local area.

In our baseline case, the delay spread for the tap delay line model of the channel can be calculated as:

$$DS^2 = \frac{1}{\sum_{l=0}^{L-1} P_l} \sum_{l=0}^{L-1} P_l \cdot (\tau_l - \bar{\tau})^2 \tag{24}$$

where

$$\bar{\tau} = \frac{1}{\sum_{l=0}^{L-1} P_l} \sum_{l=0}^{L-1} P_l \cdot \tau_l \tag{25}$$

We can write

$$DS^2 = \frac{1}{\left(\sum_{l=0}^{L-1} P_l\right)^2} \left(\left(\sum_{l=0}^{L-1} P_l\right) \cdot \left(\sum_{l=0}^{L-1} P_l \tau_l^2\right) - \left(\sum_{l=0}^{L-1} P_l \tau_l\right)^2 \right) \tag{26}$$

For simplicity, we assume that all delays τ_l are integer multiples of the same time unit T_u.

B. Single input- Single output (SISO) systems

We now assume that the receivers cannot perform any advanced signal processing: they can only sample the received signal at the appropriate instants and try to decode the transmitted signal. Instead, the system intelligence is transferred to the transmitter, that can perform prefiltering in the TR sense.

We first study the case of a single input-single output communications system, *i.e.* when $N_{TX} = 1$. For simplicity we drop the locations of the transmitter and the receiver antennas in the notation of the channel impulse response.

After the application of TR at the transmitter, the equivalent channel impulse response can be written as

$$h_{eq}(t) = h(t) \otimes \overline{h(-t)} = \sum_{l=0}^{L-1} \sum_{k=0}^{L-1} h_l \cdot \overline{h_k} \cdot \delta(t - \tau_l + \tau_k) \quad (27)$$

By symmetry

$$h_{eq}(t) = \overline{h_{eq}(-t)} \quad (28)$$

and from (27) and the assumption that $\tau_l = lT_u$

$$h_{eq}(mT_u) = \sum_{l=m}^{L-1} h_l \cdot \overline{h_{l-m}}, m \geq 0 \quad (29)$$

The equivalent channel impulse response after TR has double the temporal extent of the initial channel impulse response. It is an autocorrelation function, that is symmetric around $t = 0$, and achieves its maximum at $t = 0$.

By exploiting the properties of complex Gaussian random variables (see appendix), we can calculate the power delay profile for the equivalent channel impulse response.

$$\begin{aligned} P_{TR,0} &= E\left[|h_{eq}(0)|^2\right] &&= \left(\sum_{l=0}^{L-1} P_l\right)^2 + \sum_{l=0}^{L-1} P_l^2 \\ P_{TR,m} &= E\left[|h_{eq}(mT_u)|^2\right] &&= \sum_{l=|m|}^{L-1} P_l \cdot P_{l-|m|} \end{aligned} \quad (30)$$

We observe that

$$\begin{aligned} \sum_{m \neq 0} P_{TR,m} &= \left(\sum_{l=0}^{L-1} P_l\right)^2 - \sum_{l=0}^{L-1} P_l^2 \\ \sum P_{TR,m} &= 2\left(\sum_{l=0}^{L-1} P_l\right)^2 \end{aligned} \quad (31)$$

Therefore in the limit of large channel length L, the equivalent channel impulse response has as much power in its peak as it does in its tails. This seriously impacts the intersymbol interference (ISI) in the case of full-rate transmission. Examples of ways to combat this effect can be found in [24].

Due to the symmetry, we have $\bar{\tau} = 0$. The delay spread after TR is

$$DS^2_{TR,N_{TX}=1} = \frac{1}{\left(\sum_{l=0}^{L-1} P_l\right)^2} \sum_{m=1}^{L-1} m^2 \sum_{l=m}^{L-1} P_l P_{l-m} \quad (32)$$

Through simple manipulations, it can be shown that

$$DS = DS_{TR,N_{TX}=1} \quad (33)$$

This is a surprising result that indicates that the application of TR from a single transmit antenna does not reduce the perceived delay spread of the channel. Despite the fact that the equivalent channel impulse response appears to have more energy concentrated around $\tau = 0$, the delay spread as a 2-norm measure of its temporal extent is unaltered. However, the response is now symmetric, a property that can be exploited to simplify the design of equalizers at the receiver.

We now look at the spatial focusing properties of SISO TR. Using the fact that different taps are uncorrelated and that for complex Gaussian random variables the complex and the power correlation are related (see Appendix), it can be shown that the expected value of the interference power at a location $\mathbf{d}$ away from the intended receiver is given by

$$E\left[|IF(\mathbf{d})|^2\right] = \sum_{l=0}^{L-1} P_l^2 + \sum_{l=0}^{L-1} \sum_{k=0}^{L-1} P_l P_k \rho_{RX,l}(\mathbf{d}) \overline{\rho_{RX,k}(\mathbf{d})} \quad (34)$$

$\rho_{RX,l}(\mathbf{d})$ is the complex correlation of the l-th tap as observed at two locations separated by a distance $\mathbf{d}$. It is a function of the PAS around the receiver of this particular tap, as described in the previous section. The amount of interference depends on the power delay profile and the correlation properties of the taps. As the correlation decreases, we expect this to decrease as well. The expected peak power on the intended receiver ($\mathbf{d} = \mathbf{0}$) is given by

$$E\left[|IF(\mathbf{0})|^2\right] = \sum_{l=0}^{L-1} P_l^2 + \sum_{k=0}^{N_{TX}} \sum_{l=0}^{N_{TX}} P_l P_k \quad (35)$$

C. Multiple input- Single output (MISO) systems

We now study the case of a multiple input-single output (MISO) communications system, *i.e.* when $N_{TX} > 1$. Again the receiver samples the received signal without performing any advanced signal processing, and the transmitter performs TR prefiltering. For simplicity we drop the locations of the receiver antenna in the notation of the channel impulse response.

After the application of TR at the elements of the Tx array, the equivalent channel impulse response can be written as

$$h_{eq}(t) = \sum_{m=1}^{N_{TX}} \sum_{l=0}^{L-1} \sum_{k=0}^{L-1} h_l\left(\mathbf{r}_{TX_m}\right) \cdot \overline{h_k\left(\mathbf{r}_{TX_m}\right)} \cdot \delta(t - \tau_l + \tau_k) \quad (36)$$

Again, by symmetry $h_{eq}(t) = \overline{h_{eq}(-t)}$. The equivalent channel impulse response after TR is the sum of autocorrelation functions, and is therefore symmetric around $t = 0$. It also achieves its maximum at $t = 0$. It has double the temporal extent of the initial channel impulse responses, however we expect the autocorrelations to add coherently at $t = 0$, and incoherently off the peak. Therefore we expect the delay spread to be lower than in the baseline case and the SISO TR case.

It can be shown that

$$\begin{aligned} &P_{TR,0} = E\left[|h_{eq}(0)|^2\right] = \\ &N_{TX}^2\left(\sum_{l=0}^{L-1} P_l\right)^2 + \sum_{n=1}^{N_{TX}} \sum_{p=1}^{N_{TX}} \sum_{l=0}^{L-1} P_l^2 \left|\rho_{TX,l}(\mathbf{d}_{np})\right|^2 \end{aligned} \quad (37)$$

$$\begin{aligned} &P_{TR,m} = E\left[|h_{eq}(mT_u)|^2\right] = \\ &\sum_{n=1}^{N_{TX}} \sum_{p=1}^{N_{TX}} \sum_{l=|m|}^{L-1} P_l P_{l-|m|} \overline{\rho_{TX,l}(\mathbf{d}_{np})} \rho_{TX,l-|m|}(\mathbf{d}_{np}) \end{aligned} \quad (38)$$

where $\mathbf{d}_{np} = \mathbf{r}_{TX_n} - \mathbf{r}_{TX_p}$.

If the signals are fully correlated ($\rho_{TX,l}(\mathbf{d}_{n,p}) = 1, \forall l, n, p$), then the delay spread stays the same as in the SISO/ baseline case.

If the signals are fully decorrelated ($\rho_{TX,l}(\mathbf{d}_{n,p}) = 0, \forall\, l, n, p$), then

$$DS_{TR,N_{TX}>1} = \frac{1}{\sqrt{N_{TX}}} DS \tag{39}$$

Therefore MISO TR can reduce the delay spread by a factor of up to $\sqrt{N_{TX}}$ relative to the baseline case.

Let us now concentrate on the amount of achievable spatial focusing in the case of a MISO system. Under the assumption of Rayleigh fading and the separability of the transmit and receive correlations, it can be shown that the expected value of the interference power at a location $\mathbf{d}$ away from the intended receiver is given by

$$\begin{array}{l} E[|IF(\mathbf{d})|^2] = \\ \sum_{l=0}^{L-1} P_l^2 \sum_{n=1}^{N_{TX}} \sum_{m=1}^{N_{TX}} |\rho_{TX,l}\left(\mathbf{d}_{nm}\right)|^2 + \\ N_{TX}^2 \left[\sum_{k=0}^{L-1} \sum_{l=0}^{L-1} P_l P_k \rho_{RX,l}(\mathbf{d}) \overline{\rho_{RX,k}(\mathbf{d})}\right] \end{array} \tag{40}$$

$\rho_{RX,l}(\mathbf{d})$ is the receive correlation of the l-th tap as observed at two locations separated by a distance $\mathbf{d}$. It is a function of the PAS of the angles of arrival for this particular tap, as described in the previous section.

$\rho_{TX,l}(\mathbf{d}_{nm})$ is the transmit correlation of the l-th tap as observed at two transmitters separated by $\mathbf{d}_{nm}$. It is a function of the PAS of the angles of departure for this particular tap, as described in the previous section.

We observe that the amount of interference depends on the power delay profile and the correlation properties of the taps, at both the transmit and receive sides. As the correlation decreases, we expect this to decrease as well. The expected peak power on the intended receiver ($\mathbf{d} = \mathbf{0}$) is given by

$$\begin{array}{l} E[|IF(\mathbf{0})|^2] = \\ \sum_{l=0}^{L-1} P_l^2 \sum_{n=1}^{N_{TX}} \sum_{m=1}^{N_{TX}} |\rho_{TX,l}\left(\mathbf{d}_{nm}\right)|^2 + \\ N_{TX}^2 \sum_{k=0}^{L-1} \sum_{l=0}^{L-1} P_l P_k \end{array} \tag{41}$$

In contrast to the SISO case, the power on the target depends on the transmit correlation as well.

V. Simulation Results

Our purpose is to validate the theoretical results of the previous section, and investigate how the various parameters affect the system performance, using the 802.11n channel model.

We are going to compare three transmission scenarios, namely:

1) Baseline communications, where the receivers perform matched filtering,
2) SISO TR, where a single transmitter applies a TR filter and the receiver does not perform any equalization, and
3) MISO TR, where N_{TX} transmitters apply a TR filters and the receiver does not perform any equalization.

The channel models that we are going to investigate are the models presented in Section IIIE, namely: (a) Model B, (b) Model C, and (c) Modified Model C.

The system performance is evaluated in terms of the delay spread reduction, the achievable spatial focusing and the channel hardening.

We want to investigate how these performance measures are affected by:

- Number of transmitters: To illustrate this effect we compare the performance cases of $N_{TX} = 1$ or $N_{TX} = 2$ in an environment described by model B.
- Transmit correlation: To illustrate this effect we compare the performance of a system with two transmit antennas ($N_{TX} = 2$), separated by either 0.5λ or 2λ, in an environment that follows the description of model B.
- Delay spread of the original channel model: To illustrate this effect we compare the performance of a single transmitter system ($N_{TX} = 1$) in two environments described by model B and the modified model C respectively. These have the same angular characteristics but different delay spread characteristics.
- Angular spread at the receiver: To illustrate this effect we compare the performance of a single transmitter system ($N_{TX} = 1$) in two environments described by model C and the modified model C respectively. These have the same delay spread characteristics but different angular characteristics.

A. Illustration of time-reversal effects

Figure 3 shows the power delay profile for a channel described by model C, if no TR is applied, if TR is applied from a single transmit antenna and if TR is applied from 2 transmit antennas separated by 2λ. We observe that the application of TR doubles the temporal expent of the channel response. It also results in a clear signal peak around $\tau = 0$, that is several dB above the temporal sidelobes.

The application of TR does not completely eliminate ISI. Hence the bit error rate performance, though better than that of the original SISO channel, is impaired. This problem has already been pointed out in an underwater communication scenario [6]. In that case it can be alleviated by the existence of several transmitters (several more than would be reasonable for a wireless application) and the properties of the propagation environment.

Though not clearly visible in the figure (the scale of the plots is logarithmic), MISO TR results in lower temporal sidelobes and higher temporal focusing than its SISO counterpart, and clearly better than the original SISO channel.

B. Delay spread analysis

Table IV shows the delay spread for the three communication scenarios under investigation, and for the three channel models (Model B, Model C, and Modified Model C). The theoretical results have been derived using the definition of the delay spread (see eq. (24)) and the expected tap powers calculated analytically (see eq. (30) and (37),(38)). The simulation results are based on 200 realizations of teh channels. The theoretical and the simulation results are in good agreement.

Our first observation is that indeed SISO TR does not reduce the DS of the channel. We also observe that the larger the

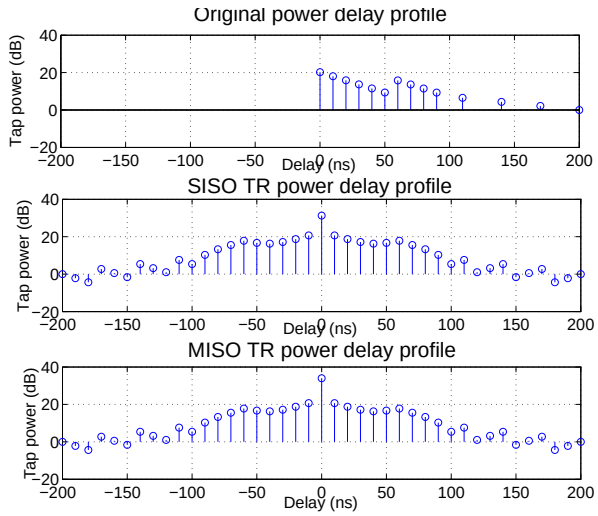

Fig. 3. Power delay profiles with and without TR for Model C

transmitter separation, the lower the transmit correlation, and therefore the greater the reduction in delay spread. Model C has wider angular spread than the Modified Model C, and therefore the transmit correlations are lower. This leads to more significant reduction of the delay spread by the application of MISO TR.

TABLE IV
RMS DELAY SPREAD COMPARISON

		Theory	Simulations
Model B	No TR	15.65ns	15.82ns
	TR ($N_{TX}=1$)	15.65ns	15.96ns
	TR ($N_{TX}=2, sep=0.5\lambda$)	14.20ns	15.41ns
	TR ($N_{TX}=2, sep=2\lambda$)	12.58ns	13.46ns
Model C	No TR	33.43ns	32.75ns
	TR ($N_{TX}=1$)	33.43ns	32.74ns
	TR ($N_{TX}=2, sep=0.5\lambda$)	27.88ns	28.52ns
	TR ($N_{TX}=2, sep=2\lambda$)	27.30ns	26.91ns
Mod. Model C	No TR	33.43ns	34.68ns
	TR ($N_{TX}=1$)	33.43ns	34.68ns
	TR ($N_{TX}=2, sep=0.5\lambda$)	30.34ns	33.42ns
	TR ($N_{TX}=2, sep=2\lambda$)	26.93ns	29.59ns

C. Spatial focusing analysis

Fig. 4 shows the expected value of the interference power around the intended receiver for Model B, assuming SISO TR, normalized by the average received power on the target, as calculated from the theoretical formulas developped in Section IV.

In order to validate the simulation process, we concentrate on an area $4\lambda \times 4\lambda$ around the intended receiver, divided into a grid of $0.2\lambda \times 0.2\lambda$ squares. We compare the simulation results with those theoretically predicted in eq. (34) and (35)). Fig. 5 and Fig. 6 show the theoretical and analytical sets of results for Model B respectively, assuming SISO TR. The limited granularity of the simulation does not allow us to see all the fineness of the interference pattern (*e.g.* the Fresnel zones). It does however reproduce the behavior of the theoretical prediction.

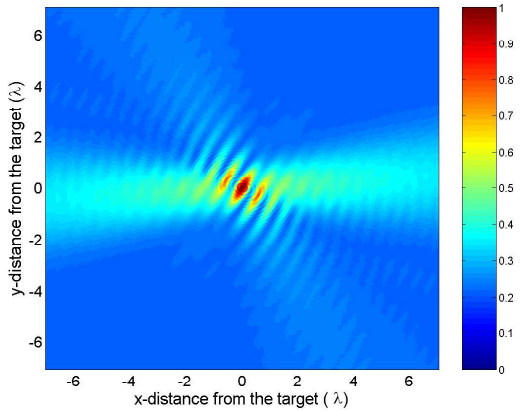

Fig. 4. Theoretical results for the spatial focusing for Model B

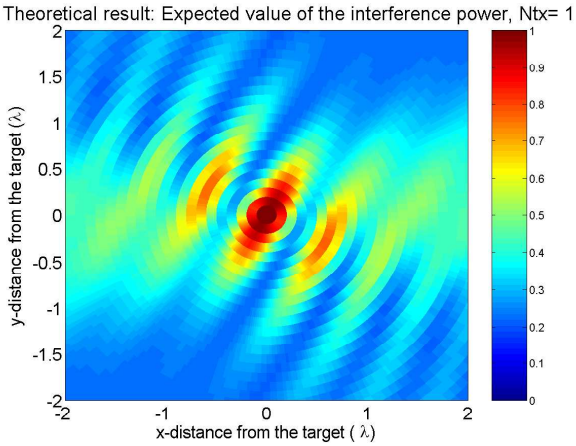

Fig. 5. Theoretically predicted average interference

The results that follow are generated by simulation and not explicit analytical calculation.

The first point that we want to make is that, in the absence of TR, no spatial focusing can be achieved. Fig. 7 shows the achievable spatial focusing in the baseline scenario (no pre-processing at the transmitter, matched-filtering at the receivers). The results shown have been generated of a channel that follows the description of Model B under the assumption of a single transmitting antenna.

The comparison with Fig. 6 shows that, if there is no preprocessing, all locations receive approximately the same amount of power, so any user within this local area can intercept and decode the transmitted signal. In that case, security and rpivacy become issues to be handled by higher layers of the communications stack. The application of TR results in a physical layer technique that achieves spatial focusing of the power on the intended receiver, and therefore both lower probability of intercept and lower interference at adjacent locations.

We now look at the effect of transmit correlation. Fig. 8 shows the spatial focusing performance when $N_{TX}=2$, and the two transmiting antenna elements are separated by either $sep=0.5\lambda$ or $sep=2\lambda$ (in the latter situation the transmit correlation is significanlty reduced).

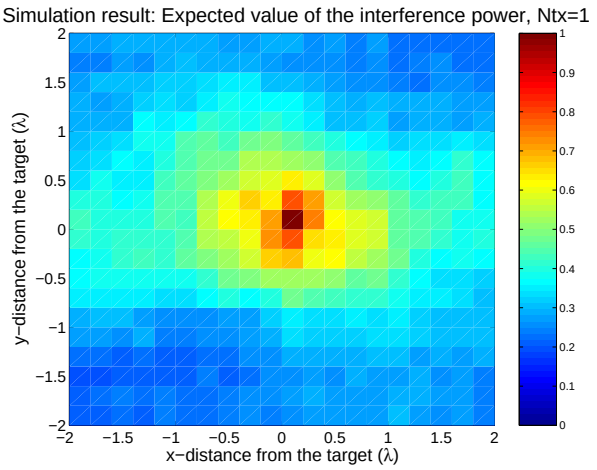

Fig. 6. Simulated interference for model B, averaged over 200 channel realizations

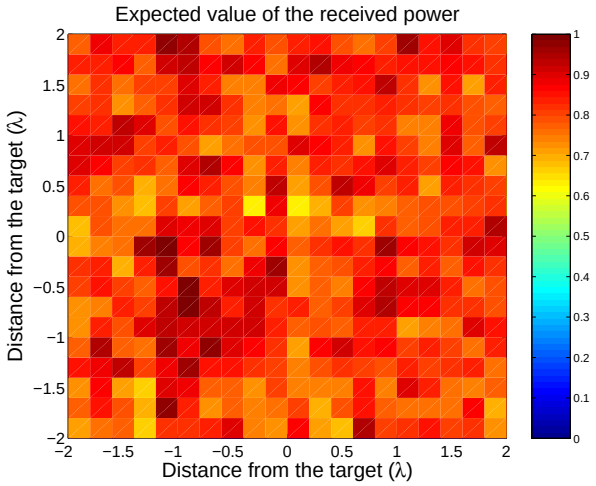

Fig. 7. Spatial focusing in the baseline scenario

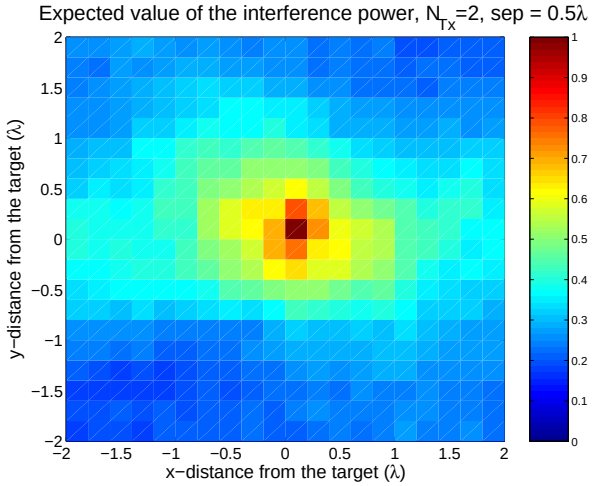

(a) MISO TR ($N_{Tx} = 2, sep = 0.5\lambda$)

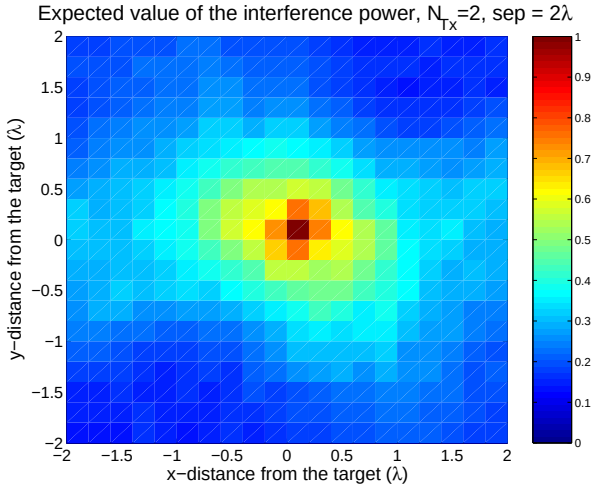

(b) MISO TR ($N_{Tx} = 2, sep = 2\lambda$)

Fig. 8. Spatial focusing in MISO TR ($N_{Tx} = 2$) (a) $sep = 0.5\lambda$, (a) $sep = 2\lambda$

The comparison of Fig. 8 with Fig. 6 shows that indeed spatial focusing improves with the introduction of more transmit elements. It does so more dramatically when the transmit elements are less correlated.

The next parameter to investigate is the delay spread of the channel. For that we compare Model B and the modified Model C that have the same angular characteristics, but different delay spreads. The comparison of 9 and Fig. 6 clearly illustrates that increasing the delay spread of the channel improves the achievable spatial focusing.

Finally, we look at how the angular spread of the channel affects the quality of the spatial focusing. For that we compare Model C and the modified Model C that have the same temporal characteristics, but different angular spreads (Model C has larger angular spread and therefore higher spatial decorrelation). The comparison of Fig. 9 and Fig. 10 clearly illustrates that increasing the angular spread of the channel improves the achievable spatial focusing. At this point it is useful to point out that the two plots decorrelate differently along the x- and y- axes. This is due to the fact that the clusters in the two models have different mean angles of arrival. The decorrelation distance is the parameter that relates to the angular spread and is the point that the plots illustrate.

D. Channel hardening

The previous section illustrated the average value of the interference power around the intended receiver and how it depends on the number of transmitters, the transmit correlation, the angular spread and the temporal spread of the channel. The question that arises is how close any realization of the channel is to the ideal performance, *i.e.* how robust the technique is to channel fading. Ideally we would like the power to focus perfectly on the intended receiver, in which case the response would be a spatial Dirac δ function. In this section we look at several realizations of the channel and compare the typical behavior to the ideal behavior, as a function of the previous

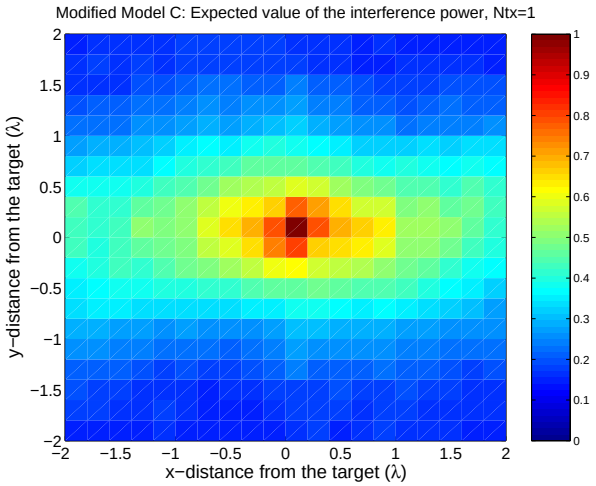

Fig. 9. Spatial focusing in SISO TR for the modified model C

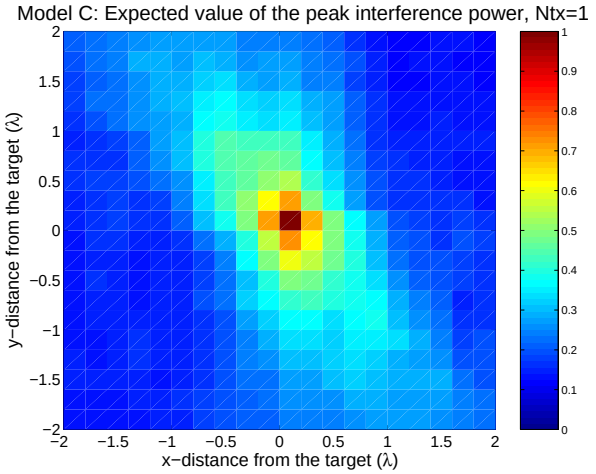

Fig. 10. Spatial focusing in SISO TR for Model C

parameters. This will give us an indication of the achievable channel hardening with TR.

Fig. 11 shows a typical channel realization from our simulations of Model C, assuming that SISO TR is applied. The comparison to the average behavior shown in Fig. 10 shows that the signal is smeared and the maxima can be displaced from the target.

We now look at how the addition of more transmit antennas and the transmit correlation impact teh channel robustness. Fig. 12(a) shows a typical realization from our simulations of a MISO TR system in channel that follows Model C, assuming that $N_{TX} = 2$ and the transmit elements are separated by $sep = 0.5\lambda$. The comparison of Fig. 11 and Fig. 12 shows that the addition of more transmit antennas helps stabilize the spatial focusing of a TR system. Moreover, Fig. 12(b) shows a typical realization from our simulations of a MISO TR system in channel that follows Model C, assuming that $N_{TX} = 2$ and the transmit elements are separated by $sep = 2\lambda$, and are therefore less correlated. By comparing Fig. 12(a) and Fig. 12(b) we observe that when the transmit elements are less correlated, the spatial focusing becomes more robust.

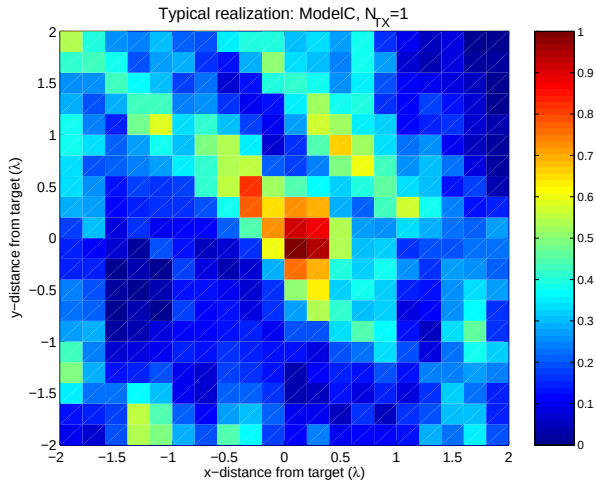

Fig. 11. Typical spatial focusing in SISO TR for Model C, $N_{TX} = 1$

Our target now is to investigate the effect of angular diversity. Fig. 13 shows a typical realization of spatial focusing assuming that the channel follows the modified Model C, *i.e.* has the same delay spread characteristics as Model C, but more narrow angular spread characteristics. The comparison of Fig. 13 and Fig. 11 shows that the additional angular diversity in Model C enhances the spatial focusing by limiting the number of displaced maxima. This relates to the enhanced triangulation properties that can be achieved with wider angular spread.

Finally, our target is to investigate the effect of delay spread. Fig. 14 shows the worst-case spatial focusing assuming that the channel follows Model B, *i.e.* has the same angular spread characteristics as the modified Model C, but smaller delay spread. The comparison of Fig. 13 and Fig. 14 shows that delay spread enhances the spatial focusing by limiting the spatial side-lobes.

VI. Conclusions

In this paper, we investigated analytically and demonstrated with simulations the spatio-temporal focusing potential of the time-reversal technique and how it relates to the channel properties.

We showed that the application of the TR techniques does not reduce the perceived delay spread of the channel in the SISO situation (see 33). In that case, additional signal processing at the receiver and/ or transmitter is required. The addition of more transmit antennas can reduce the delay spread of the channel. The effectiveness of this technique depends on the channel correlation around the transmitters (see (39)).

The spatial focusing properties of TR depend on the channel correlation around the intended receiver in both the SISO and MISO TR situations (see (34) and (41)).

The theoretical results were verified by detailed simulations of the 802.11n channel model, that describes typical situations in wireless local area network (WLAN) scenarios. The channel model reflects a concensus of the WLAN community, which lends credibility to the propagation situations it outlines. The simulation results showed very good agreement with the

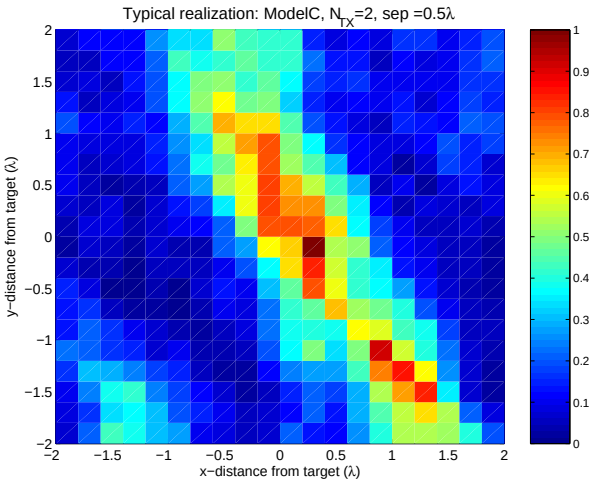

(a) MISO TR ($N_{Tx} = 2, sep = 0.5\lambda$)

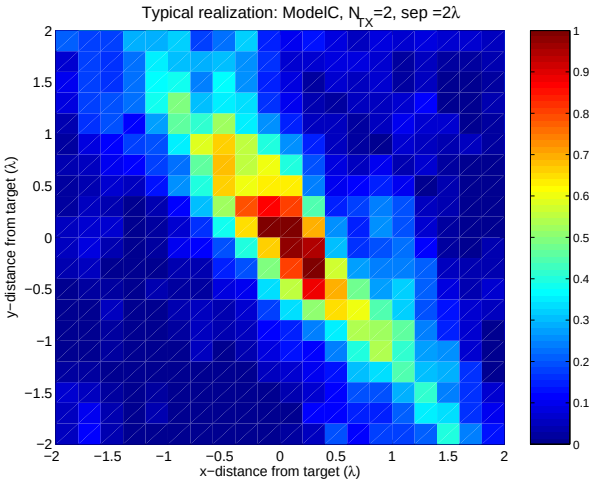

(b) MISO TR ($N_{Tx} = 2, sep = 2\lambda$)

Fig. 12. Typical spatial focusing in MISO TR for Model C, ($N_{Tx} = 2$) (a) $sep = 0.5\lambda$, (a) $sep = 2\lambda$

analytical results. They also illustrated that increased delay spread, increased angular spread, more transmit elements and low transmit correlations contribute to robust spatial focusing.

The results that we illustrated in this paper involve the theoretical investigation of the temporal and spatial focusing properties of TR in an indoor wireless local area network scenario. To experimentally demonstrate the validity of these results, a channel sounding experiment is required. Indeed, the Smart Antennas Research Group at Stanford University will perform such an experiment using a mutliple antenna wide-band channel sounder (8 receive elements, $B = 200MHz$).

ACKNOWLEDGMENT

The work of P. Kyritsi and G. Papanicolaou was supported partially by grants NSF: DMS-0354674-001 and ONR: N00014-02-1-0088.

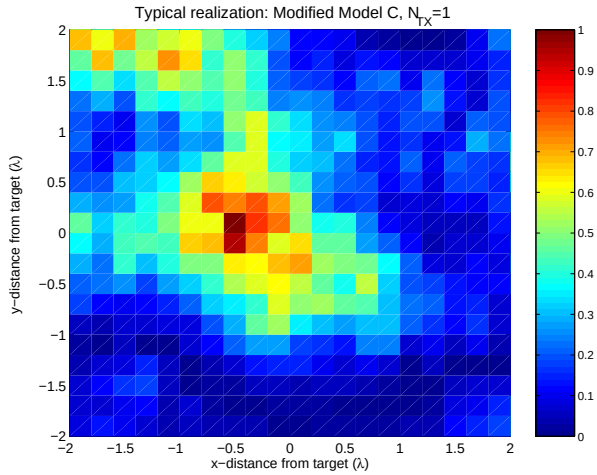

Fig. 13. Typical spatial focusing in SISO TR for the modified Model C

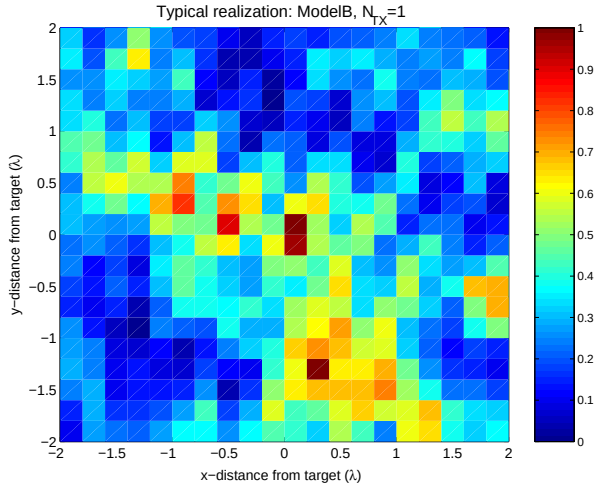

Fig. 14. Typical spatial focusing in SISO TR for Model B

APPENDIX

The following properties of Gaussian random variables are useful for the derivation of the analytical properties in this paper.

- Higher order moments
  If x is a real, zero-mean, Gaussian random variable with variance σ^2, then

$$\begin{aligned} E[x^2] &= \sigma^2 \\ E[x^4] &= 3\sigma^4 \end{aligned} \tag{42}$$

  If u is a complex, circularly symmetric, zero-mean, Gaussian random variable with variance σ^2, then

$$\begin{aligned} E[|x|^2] &= \sigma^2 \\ E[|x|^4] &= 2\sigma^4 \end{aligned} \tag{43}$$

- Power and complex correlations
  Let x, y be two complex Gaussian random variables.

Their complex correlation is defined as

$$\rho^{IQ}(x,y) = \frac{E\left[\overline{x}y\right] - E\left[\overline{x}\right]E\left[y\right]}{\sqrt{\left(E\left[|x|^2\right] - |E\left[x\right]|^2\right)\left(E\left[|y|^2\right] - |E\left[y\right]|^2\right)}} \quad (44)$$

and their power correlation is defined as

$$\rho^{PWR}(x,y) = \frac{E\left[P_x P_y\right] - E\left[P_x\right]E\left[P_y\right]}{\sqrt{\left(E\left[P_x^2\right] - E\left[P_x\right]^2\right)\left(E\left[P_y^2\right] - E\left[P_y\right]^2\right)}} \quad (45)$$

where $P_x = |x|^2$, $P_y = |y|^2$.
The power and complex correlations are related by

$$\rho^{PWR}(x,y) = \left|\rho^{IQ}(x,y)\right|^2 \quad (46)$$

- Product of Gaussians
  Let x_1, x_2, x_3, x_4 be zero-mean, real Gaussian random variables, with covariance matrix C. This means that

$$C_{ij} = E\left[x_i x_j\right] \quad (47)$$

The expectation of the product $x_1x_2x_3x_4$ is given by

$$E\left[x_1x_2x_3x_4\right] = C_{12}C_{34} + C_{13}C_{24} + C_{14}C_{23} \quad (48)$$

REFERENCES

[1] M. Fink, "Time reversed acoustics," *Physics Today*, March, pp. 33-40, 1997.

[2] M. Fink, "Time-reversed acoustics," *Scientific American*, November, pp. 91-97, 1999.

[3] M. Fink, D. Cassereau, A. Derode, C. Prada, P. Roux, M. Tanter, J-L. Thomas and F. Wu, "Time-reversed acoustics," *Reports on Progress in Physics*, vol. 63, pp. 1933-1995, 2000.

[4] W. A. Kuperman, W. S. Hodgkiss, H. C. Song, T. Akal, C. Ferla, and D. R. Jackson, "Phase conjugation in the ocean: Experimental demonstration of a time reversal mirror," *J. Acoust. Soc. Am.*, vol. 103, pp. 25-40, 1998.

[5] G. Lerosey, J. de Rosny, A. Tourin, A. Derode, G. Montaldo, and M. Fink, "Time Reversal of electromagnetic waves," in *Physical Review Letters*, no 92, 2004.

[6] D. Rouseff, "Intersymbol interference in underwater acoustic communications using time-reversal signal processing," in *J. Acoust. Soc. Am.*, vol. 117, pp. 780-788, 2005.

[7] P. Kyritsi, G. Papanicolaou, P. Eggers and A. Opera, "MISO time reversal and delay spread compression for FWA channels at 5 GHz," *Antennas and Wireless Propagation Letters* vol. 3, pp. 96-99, 2004.

[8] P. Kyritsi, G. Papanicolaou, P. Eggers, and A. Oprea, "Time reversal techniques for wireless communications," in *Proc. IEEE 60th Vehicular Technology Conference*, Sept. 2004, vol. 1, pp. 47-51.

[9] W. S. Hodgkiss, H. C. Song, W. A. Kuperman, T. Akal, C. Ferla and D. R. Jackson, "A long-range and variable focus phase-conjugation experiment in shallow water," *J. Acoust. Soc. Am.*, vol. 105, pp. 1597-1604, 1999.

[10] S. Kim, G. Edelmann, W. S. Hodgkiss, W. A. Kuperman, H. C. Song, and T. Akal, "Spatial resolution of time reversal array in shallow water," *J. Acoust. Soc. Am.*, vol. 110, pp. 820-829, 2001.

[11] G. Edelmann, T. Akal, W. S. Hodgkiss, S. Kim, W. A. Kuperman, H. C. Song, "An initial demonstration underwater acoustic communication using time reversal," *IEEE J. of Oceanic Eng.*, vol. 27, pp. 602-609, 2002.

[12] S. Kim, W. A. Kuperman, W. S. Hodgkiss, H. C. Song, G. Edelmann, and T. Akal, "Robust time reversal focusing in the ocean," *J. Acoust. Soc. Am.*, vol. 114, pp. 145-157, 2003.

[13] D. Rouseff, "Intersymbol interference in underwater acoustic communications using time-reversal signal processing," submitted to *J. Acoust. Soc. Am.*, 2004.

[14] C. Oestges, A. D. Kim, G. Papanicolaou, A. J. Paulraj, "Characterization of space-time focusing in time-reversed random fields," in *IEEE Trans. Antennas Propagat.*, vol. 5, pp. 283-293, 2005.

[15] J. G. Proakis, *Digital Communications* 4th ed. McGraw-Hill, New York, 2001.

[16] W.C. Jakes, *Microwave Mobile Communications*, IEEE Press Reprints, New Jersey, 1994.

[17] A. Kim, P. Kyritsi, P. Blomgren, and G. Papanicolaou, "Low probability of intercept and intersymbol interference in multiple-input/ single-output time reversal communication systems," submitted to *IEEE Journal of Oceanic Engineering*, Nov. 2004.

[18] J.P. Kermoal, L. Schumacher, K.I. Pedersen, P.E. Mogensen, and F. Frederiksen, "A stochastic MIMO radio channel model with experimental validation," *IEEE Journal on Selected Areas in Communications*, vol. 20 , no 6, pp. 1211-1226, Aug. 2002.

[19] L. Schumacher, K.I. Pedersen, and P.E. Mogensen, "From antenna spacings to theoretical capacities - guidelines for simulating MIMO systems," in Proc. 13th IEEE International Symposium on Personal, Indoor and Mobile Radio Communications, 2002, vol. 2, pp. 587-592.

[20] J. Chuang, "The Effects of Time Delay Spread on Portable Radio Communications Channels with Digital Modulation," in *IEEE Journal on Selected Areas in Communications*, Vol. 5, no. 5, June 1987, pp. 879 -889.

[21] H. Ozcelik, M. Herdin, W. Weichselberger, J. Wallace, and E. Bonek, "Deficiencies of 'Kronecker' MIMO radio channel model," in *Electronics Letters*, vol. 39, no. 16, 7 Aug. 2003, pp. 1209-1210.

[22] V. Erceg, L. Schumacher, P. Kyritsi, A. Molisch, D.S. Baum, et al. "TGn channel models," IEEE 802.11-03/940r2, Jan. 2004.

[23] L. Schumacher, and B. Dijkstra, "Description of a MATLAB implementattion of the indoor MIMO WLAN channel model proposed by the IEEE 802.11 TGn channel model special committee", ftp://ieee:wireless@ftp.802wirelessworld.com/11/03/11-03-0940-04-000n-tgn-channel-models.doc

[24] M. Emami, M. Vu, J. Hansen, A. Paulraj, and G. Papanicolaou, "Matched Filtering with Rate Back-off for Low Complexity Communications in Very Large Delay Spread Channels", in Proc. Asilomar Conference on Signals, Systems, and Computers, Nov. 2004.

[25] M. Emami, J. Hansen, A.D. Kim, G. Papanicolaou, A.J. Paulraj, D. Cheung, and C. Prettie, "Predicted Time Reversal Performance in Wireless Communications Using Channel Measurements," accepted for publication in *IEEE Communications Letters.*

[26] T. Strohmer, M. Emami, J. Hansen, G. Papanicolaou, and A. Paulraj, "Application of time-reversal with MMSE equalizer to UWB communications," in Proc. IEEE Global Telecommunications Conference, 2004, Vol. 5, pp. 3123 - 3127.

[27] B.E. Henty, D.D. Stancil, "Multipath-enabled super-resolution for rf and microwave communications using phase-conjugate arrays," in *Physical Review Letters*, no 93, December 2004.

[28] J. Medbo and P. Schramm, "Channel models for HIPERLAN/2," ETSI/BRAN document no. 3ERI085B.

[29] J. Medbo and J-E. Berg, "Measured radiowave propagation characteristics at 5 GHz for typical HIPERLAN/2 scenarios," ETSI/BRAN document no. 3ERI084A.

[30] A.A.M. Saleh and R.A. Valenzuela, "A statistical model for indoor multipath propagation," in *IEEE J. Select. Areas Commun.*, vol. 5, 1987, pp. 128-137.

[31] Q.H. Spencer, et al., "Modeling the statistical time and angle of arrival characteristics of an indoor environment," in *IEEE J. Select. Areas Commun.*, vol. 18, no. 3, March 2000, pp. 347-360.

[32] Chia-Chin Chong, D.I. Laurenson and S. McLaughlin, "Statistical Characterization of the 5.2 GHz wideband directional indoor propagation channels with clustering and correlation properties," in Proc. IEEE Veh. Technol. Conf., vol. 1, Sept. 2002, pp. 629-633.

Persefoni Kyritsi received the B.S. degree in electrical engineering from the National Technical University of Athens, Athens, Greece, in 1996, the M.S. and the Ph.D. degrees in Electrical Engineering from Stanford University, Stanford, CA, in 1998 and 2002 respectively. She has spent time as an intern with Lucent Technologies Bell Labs, Deutsche Telekom, Intel and Nokia. Since 2001, she has been with the Department Communication Technology in Aalborg University, Aalborg, Denmark, as an Assistant Research Professor. Currently, she is on a leave of absence from Aalborg a nd is working as a post-doctoral researcher at the Department of Mathematics at Stanford University.

George Papanicolaou received his PhD in Mathematics in 1969 from the Courant Institute of New York University. He joined the faculty of the Courant Institute where he was professor from 1976-1993. He has been professor of Mathematics at Stanford University since 1993.